

HYDRAULIC FORCES CAUSED BY ANNULAR PRESSURE SEALS IN CENTRIFUGAL PUMPS

T.Iino and H.Kaneko
Mechanical Engineering Research Laboratory, Hitachi,Ltd.
Tsuchiura, Japan

SUMMARY

An experimental study was performed with static and dynamic test apparatus to investigate the hydraulic forces caused by annular pressure seals. The measured inlet and exit loss coefficients of the flow through the seals were much smaller than the conventional values, though the measured resistance coefficients agreed well with the values calculated by the equations proposed by Yamada and by Tao and Donovan. The results of the dynamic tests showed that the damping coefficient and the inertia coefficient of the fluid film in the seal were not affected much by the rotational speed or the eccentricity of the rotor, though the stiffness coefficient seemed to be influenced by the eccentricity.

INTRODUCTION

It has been reported that annular pressure seals in centrifugal pumps have great influence on the lateral vibrations of the shaft systems (ref. 1 and 2). In order to analyze the dynamic properties of the fluid films in the annular seals, it is necessary to know the boundary conditions of pressure such as pressure at the both ends of the seal. It is also important to evaluate properly the resistance coefficient of the flow in the seal both in the axial and the circumferential directions. Unfortunately there are few data available to evaluate those values, especially when the configuration of the seal is complicated.

In this study two series of experiments, static tests and dynamic tests, are carried out. In the static tests, pressure distributions in the eccentric seals are measured under several conditions of the eccentricity, the axial pressure difference and the speed of the rotor to investigate the inlet and the exit loss coefficients and the resistance coefficients, which will help the dynamic analysis.

Then the dynamic forces at the seals caused by a vibrating rotor are measured. The dynamic properties of the fluid films in the seals are calculated from the test results.

NOMENCLATURE

The following nomenclature is used in the paper:

c	damping coefficient, N·s/m
d	seal diameter, m
e	eccentricity ratio ($=\delta/G$)
f	static force on an eccentric rotor, N
\bar{F}	non-dimensional force on the rotor ($=f/(0.5\rho\cdot v_m^2\cdot d\cdot l)$)
F	dynamic force on the stator, N
G	seal clearance when concentric, m
k	stiffness coefficient, N/m
l	seal width, m
m	inertia coefficient, N·s ² /m
N	rotational speed, rps
p	pressure, N/m
\bar{p}	non-dimensional pressure ($=(p-p_6)/(p_1-p_6)$)
$\Delta\bar{p}_{max}$	non-dimensional maximum pressure difference in a section perpendicular to the axis ($=(p_{max}-p_{min})_{x=x}/(p_{max}-p_{min})_{x=0}$)
Q	leakage flow rate, m ³ /s
R_a	axial Reynolds number ($=v_m\cdot G/\nu$)
R_r	rotational Reynolds number ($=\pi\cdot d\cdot N\cdot G/\nu$)
v	axial velocity component of the flow in the seal, m/s
v_m	mean axial velocity ($=Q/(\pi\cdot d\cdot G)$), m/s
x	co-ordinate in the axial direction ($x=0$ at the inlet of the seal), m
X	rotor displacement in the vertical direction, m
Y	rotor displacement in the horizontal direction, m
δ	eccentricity, m
θ	co-ordinate in the circumferential direction ($\theta=0$ at the top of the seal)
λ	resistance coefficient ($dp=\lambda\cdot(dx/2G)\cdot(\rho\cdot v_m^2/2)$)
λ_0	resistance coefficient proposed by Yamada ($=0.26R_a\{1+(7/8)\cdot(R_r/2R_a)^2\}^{0.38}$)
ν	kinematic viscosity, m ² /s
ξ_{in}	inlet loss coefficient ($=(p_1-p_2)/(0.5\rho\cdot v_m^2)-\lambda\cdot x_2/(2G)-1$)
ξ_{out}	exit loss coefficient ($=1-(p_6-p_4)/(0.5\rho\cdot v_m^2)-\lambda\cdot(1-x_4)/(2G)$)
ρ	density, kg/m
ω	vibration angular velocity, rad/s

Subscripts:

0	amplitude at the frequency given by the vibrator
1-6	value at the measuring position 1-6
1-3	value corresponding to the vibration angular velocity $\omega, -\omega$
X	component in the vertical direction
Y	component in the horizontal direction
XX, XY, YX, YY	used in the dynamic properties of the fluid film; The first subscript denotes the direction of the force. The second subscript denotes the direction of the displacement, velocity or acceleration.

STATIC TEST APPARATUS

The static test apparatus is shown in figure 1. Static pressure was measured at the pressure holes distributed at six axial positions and eight circumferential positions with pressure transducers of strain gauge type. The eccentricity of the rotor was measured with displacement sensors of eddy current type at two axial positions and two circumferential positions, 90 degree apart from each other. The radial load on the bearings in the both vertical and horizontal directions were also measured with load transducers of strain gauge type. The static pressure in the high and low pressure chambers were measured as well as the flow rate through the seals.

Tests were performed under conditions of the axial Reynolds number R_a between 1100 and 3500 and the rotational Reynolds number R_r between 0 and 4800.

TEST SEALS

The configurations of test seals are shown in figure 2. The seals have relatively small ratio of width to diameter. Figure 2 also shows the axial positions of the pressure holes 1 to 6 and the axial positions of the displacement sensors A and B.

TEST RESULTS

Figure 3 shows a typical pressure distribution measured in the test seal I. It is noted that the maximum pressure in a section perpendicular to the axis was measured near the circumferential position where the clearance was minimum throughout the whole width of the seal. It was the same regardless of the pressure difference or the rotor speed, provided that the ratio of the width to diameter of the seal was small and that the seal had grooves just like the seals I and III shown in figure 2.

It should also be noted that even at the position 5 behind the seal exit, considerable pressure difference in the circumferential direction still remained. This result implies that it is not appropriate to the analysis of the flow to assume that the pressure at the exit of the seal is uniform and equal to the pressure in the low pressure chamber.

Figure 4 shows the maximum pressure difference $\overline{\Delta p_{max}}$ in the section perpendicular to the axis. In the case of the flat seal (test seal II) $\overline{\Delta p_{max}}$ decreased linearly in the axial direction. On the other hand, in the case of the grooved seals (test seals I and III) $\overline{\Delta p_{max}}$ had the minimum value and then increased again.

Figure 5 shows the influence of the inclination between the axes of the rotor and the stator on the pressure distributions in the seal. The effect of the inclination can not be neglected, especially when the eccentricity is large.

Figures 6 and 7 show the inlet and the exit loss coefficients respectively calculated from the pressure distributions. The inlet loss coefficient ξ_{in} was much smaller than the conventional value, 0.5. The exit loss coefficient ξ_{out} was also considerably smaller than the conventional value, 1.0. Since the pressure at the exit is expressed by the equation

$$p(\theta) = p_0 - (1 - \xi_{out}) \cdot \rho \cdot v(\theta)^2 / 2 \quad (1)$$

small ξ_{out} gives a reasonable explanation to the pressure distribution there. According to the experimental results by Stampa (ref. 3), inlet and exit loss coefficients are strongly affected by the axial and the rotational Reynolds numbers. Within the range of the Reynolds numbers of the experiments presented here, the rotational Reynolds number did not have much influence on the inlet loss coefficient, though it had some influence on the exit loss coefficient.

Figure 8 shows the resistance coefficient λ calculated from the pressure distribution. It was normalized by λ_0 , which was calculated by the equation proposed by Yamada for concentric flat seals (ref. 4). The experimental resistance coefficient λ for the flat seal agreed well with the coefficient calculated by Yamada's equation with consideration for the effect of eccentricity analyzed by Tao and Donovan (ref. 5).

Figure 9 shows the non-dimensional radial forces calculated from the measured pressure distributions. In the case of the test seals I and II, the radial forces did not depend much on the Reynolds numbers in these experiments. On the other hand in the case of the test seal III, the ratio of the rotational Reynolds number to the axial one had considerable influence on the forces. It is noted that the flow resistance in the circumferential direction is large in the flat seal and the rotor revolution has considerable effect on the flow in the eccentric flat seals.

DYNAMIC TEST APPARATUS

Figure 10 shows the dynamic test apparatus. The shaft was vibrated vertically by a hydraulic vibrator. Vertical and horizontal relative vibrations between the rotor and the stator of the test seal were measured at two axial positions with displacement sensors of eddy current type. Vertical and horizontal forces acting on the stator were measured at two axial positions with load sensors of strain gauge type.

TEST DATA PROCESSING

Test data were recorded on magnetic tapes and analyzed with a computer.

First the analogue signals were converted into digital signals with a high speed AD converter. Then the digital signals were processed by the digital filter method and the amplitudes and the phases at the frequency given by the vibrator were calculated. Vibration amplitudes at two axial positions were averaged to be used in the farther processing. Load amplitudes at two axial positions were added to each other to obtain the total values. The acceleration of the casing was also measured and was taken into account to correct the load amplitudes. The amplitudes and the phases were transformed into the real and the imaginary parts of complex expressions.

The relations between the dynamic properties of the fluid film and the hydraulic forces acting on the stator are expressed by the following equations.

$$\begin{aligned} m_{xx}\ddot{X} + m_{xy}\ddot{Y} + c_{xx}\dot{X} + c_{xy}\dot{Y} + k_{xx}X + k_{xy}Y &= F_x \\ m_{yx}\ddot{X} + m_{yy}\ddot{Y} + c_{yx}\dot{X} + c_{yy}\dot{Y} + k_{yx}X + k_{yy}Y &= F_y \end{aligned} \quad (2)$$

The vibrations of the rotor and the forces on the stator may be expressed in the complex number as follows.

$$\begin{aligned} X &= X_0 e^{i\omega t} = \{ \text{Re}(X_0) + i\text{Im}(X_0) \} e^{i\omega t} \\ Y &= Y_0 e^{i\omega t} = \{ \text{Re}(Y_0) + i\text{Im}(Y_0) \} e^{i\omega t} \\ F_x &= F_{x0} e^{i\omega t} = \{ \text{Re}(F_{x0}) + i\text{Im}(F_{x0}) \} e^{i\omega t} \\ F_y &= F_{y0} e^{i\omega t} = \{ \text{Re}(F_{y0}) + i\text{Im}(F_{y0}) \} e^{i\omega t} \end{aligned} \quad (3)$$

Since only four equations are obtained for twelve unknowns m_{xx} , m_{xy} , m_{yx} , m_{yy} , c_{xx} , c_{xy} , c_{yx} , c_{yy} , k_{xx} , k_{xy} , k_{yx} and k_{yy} for each vibration frequency, three experiments at different vibration frequencies are necessary to obtain full equations. The final equations are expressed in the matrix form as follows.

$$\begin{bmatrix} \text{Re}(X_{01}) & \text{Re}(Y_{01}) & -\omega_1 \text{Im}(X_{01}) & -\omega_1 \text{Im}(Y_{01}) & -\omega_1^2 \text{Re}(X_{01}) & -\omega_1^2 \text{Re}(Y_{01}) \\ \text{Re}(X_{02}) & \text{Re}(Y_{02}) & -\omega_2 \text{Im}(X_{02}) & -\omega_2 \text{Im}(Y_{02}) & -\omega_2^2 \text{Re}(X_{02}) & -\omega_2^2 \text{Re}(Y_{02}) \\ \text{Re}(X_{03}) & \text{Re}(Y_{03}) & -\omega_3 \text{Im}(X_{03}) & -\omega_3 \text{Im}(Y_{03}) & -\omega_3^2 \text{Re}(X_{03}) & -\omega_3^2 \text{Re}(Y_{03}) \\ \text{Im}(X_{01}) & \text{Im}(Y_{01}) & \omega_1 \text{Re}(X_{01}) & \omega_1 \text{Re}(Y_{01}) & -\omega_1^2 \text{Im}(X_{01}) & -\omega_1^2 \text{Im}(Y_{01}) \\ \text{Im}(X_{02}) & \text{Im}(Y_{02}) & \omega_2 \text{Re}(X_{02}) & \omega_2 \text{Re}(Y_{02}) & -\omega_2^2 \text{Im}(X_{02}) & -\omega_2^2 \text{Im}(Y_{02}) \\ \text{Im}(X_{03}) & \text{Im}(Y_{03}) & \omega_3 \text{Re}(X_{03}) & \omega_3 \text{Re}(Y_{03}) & -\omega_3^2 \text{Im}(X_{03}) & -\omega_3^2 \text{Im}(Y_{03}) \end{bmatrix} \begin{bmatrix} k_{xx} \\ k_{xy} \\ c_{xx} \\ c_{xy} \\ m_{xx} \\ m_{xy} \end{bmatrix} = \begin{bmatrix} \text{Re}(F_{x01}) \\ \text{Re}(F_{x02}) \\ \text{Re}(F_{x03}) \\ \text{Im}(F_{x01}) \\ \text{Im}(F_{x02}) \\ \text{Im}(F_{x03}) \end{bmatrix} \quad (4)$$

Only six equations for the equilibrium of the forces in the X direction are shown here. The equations in the Y direction are obtained by replacing the unknown vector and the vector in the right hand side.

TEST SEAL AND TEST RESULTS

A test seal similar to the test seal I in figure 2 was set in the apparatus and tested.

Figure 11 shows typical test data. Six vibration frequencies from 10 to

40 Hz were selected. The vibration amplitude $R_e(X_c)$ was set around $12 \mu\text{m}$ (7% of the seal clearance) and $I_m(X_c)$ and Y_c were very small regardless of the vibration frequency.

$R_e(F_{xc})/R_e(X_c)$ decreased parabolically with the increase in the vibration frequency because in these experiments $R_e(F_{xc})/R_e(X_c) \doteq k_{xx} - \omega^2 \cdot m_{xx}$. On the other hand $I_m(F_{xc})/R_e(X_c)$ increased linearly with the vibration frequency because $I_m(F_{xc})/R_e(X_c) \doteq \omega \cdot c_{xx}$.

Figure 12 shows some results of dynamic properties of the fluid film in the seal. The pressure difference across the seal was maintained nearly constant. The time-averaged eccentricity of the rotor changed with the rotational speed. Damping coefficient c_{xx} and inertia coefficient m_{xx} did not change much with the speed or the eccentricity within the experimental range of the parameters. Stiffness coefficient k_{xx} changed considerably with the speed. From the results of the static test (fig. 9) this change in k_{xx} is considered to be the effect of the eccentricity rather than the effect of the speed.

CONCLUDING REMARKS

An experimental study was performed with static and dynamic test apparatus to investigate the hydraulic forces caused by annular pressure seals. The following conclusions are deduced.

1. The pressure at the exit of the seal had considerable variation in the circumferential direction.
2. The inclination between the axes of the rotor and the stator had much influence on the pressure distribution in the seal.
3. The inlet loss coefficient was much smaller than the conventional value, 0.5. It was affected by the axial Reynolds number.
4. The exit loss coefficient was smaller than the conventional value, 1.0. This result gives a reasonable explanation to the conclusion 1.
5. The experimental resistance coefficient for the flat seal agreed well with the coefficient calculated by Yamada's equation with consideration for the effect of eccentricity analyzed by Tao and Donovan.
6. The hydraulic forces caused by the eccentricity of the rotor had strong non-linearity to the eccentricity.
7. The results of the dynamic test showed that the damping coefficient c_{xx} and the inertia coefficient m_{xx} were not affected much by the rotational speed or the eccentricity of the rotor, though the stiffness coefficient k_{xx} seemed to be influenced by the eccentricity.

REFERENCES

1. Black, H.F. and Jenssen, D.N., "Effects of Pressure Ring Seals on Pump Rotor Vibration," ASME Paper, No.71-WA/FE-38, 1970.
2. Makay, E., "Eliminating Pump Stability Problems," Power, July 1970.
3. Stampa, B., "Experimentelle Untersuchungen an axial durchströmten Ringspalten," Ph.D. Thesis, Technischen Universität Carolo-Wilhelmina, Braunschweig, 1971.
4. Yamada, Y., "Resistance of a Flow through an Annulus with an Inner Rotating Cylinder," Bulletin of the Japan Society of Mechanical Engineers, Vol.5, No.18, May 1962.
5. Tao, L.N. and Donovan, W.F., "Through-Flow in Concentric and Eccentric Annuli of Fine Clearance with and without Relative Motion of the Boundaries," Trans. ASME, Vol.77, November 1955.

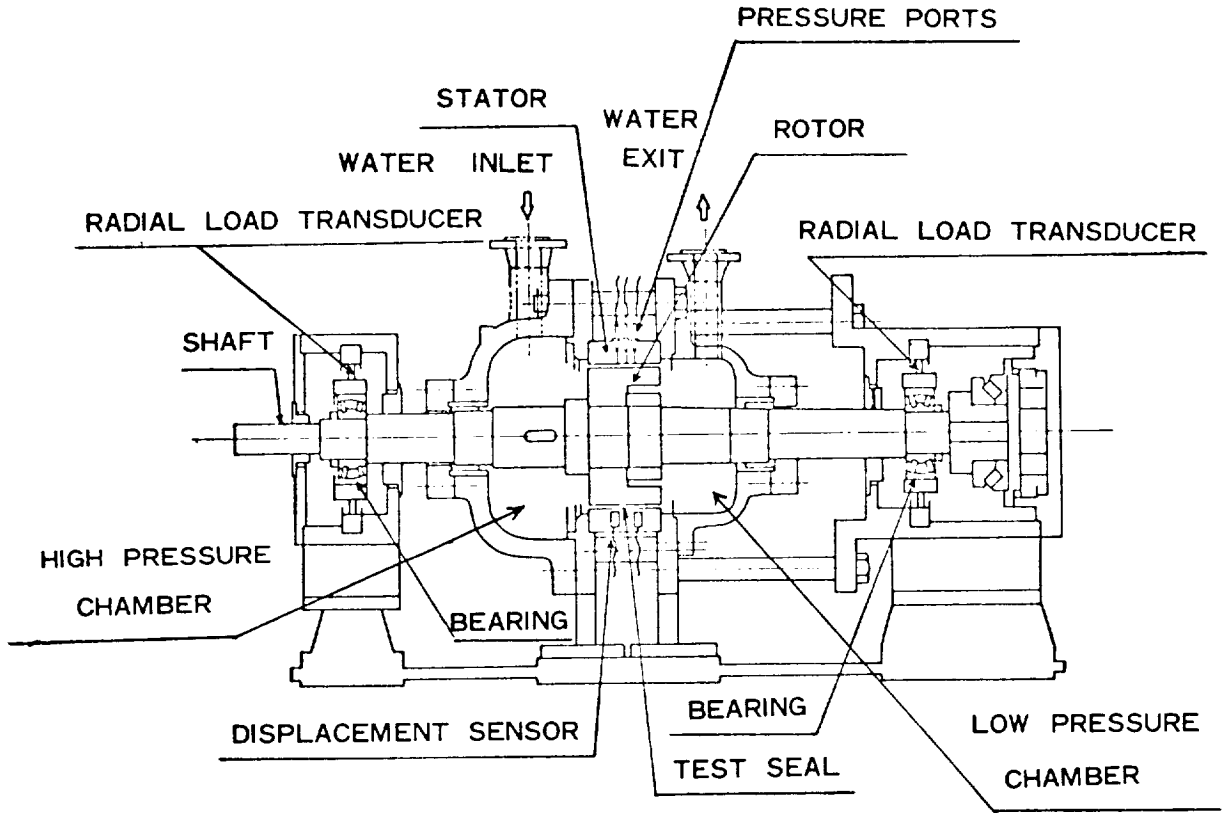


Figure 1. Static test apparatus

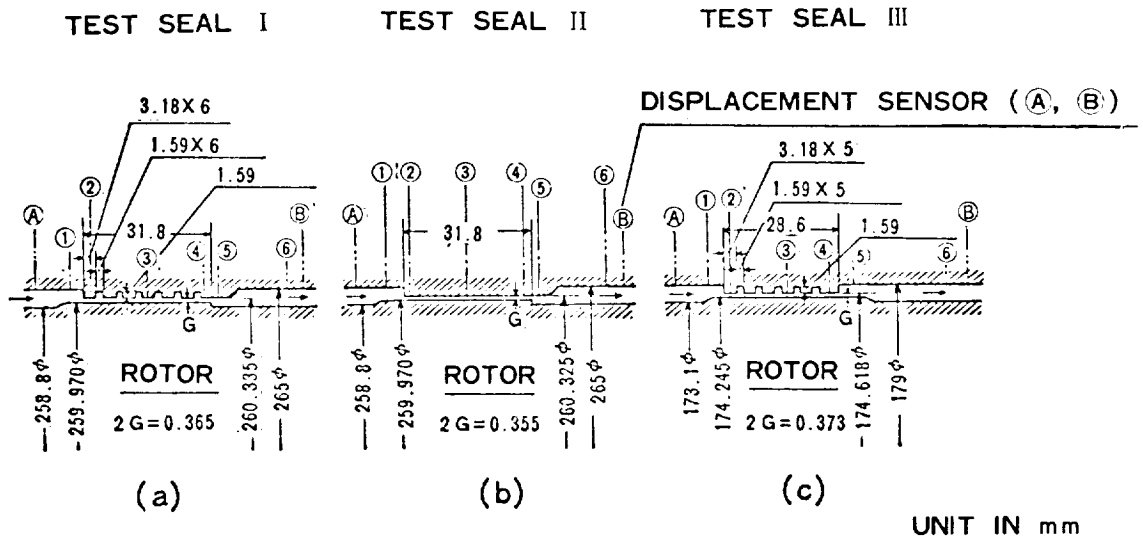


Figure 2. Test seals

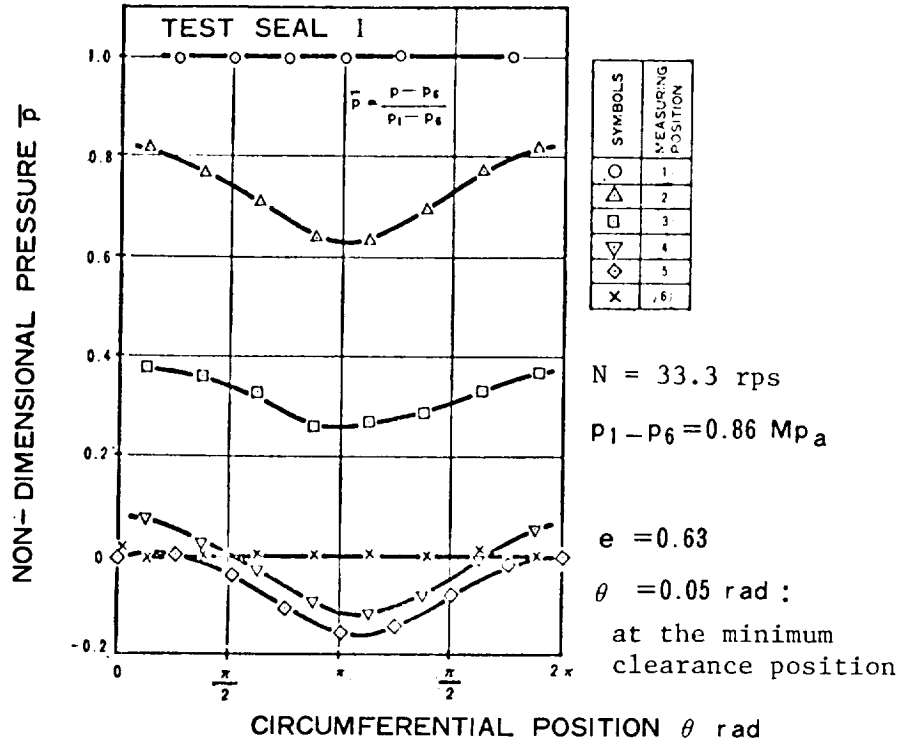


Figure 3. Pressure distribution in an eccentric seal

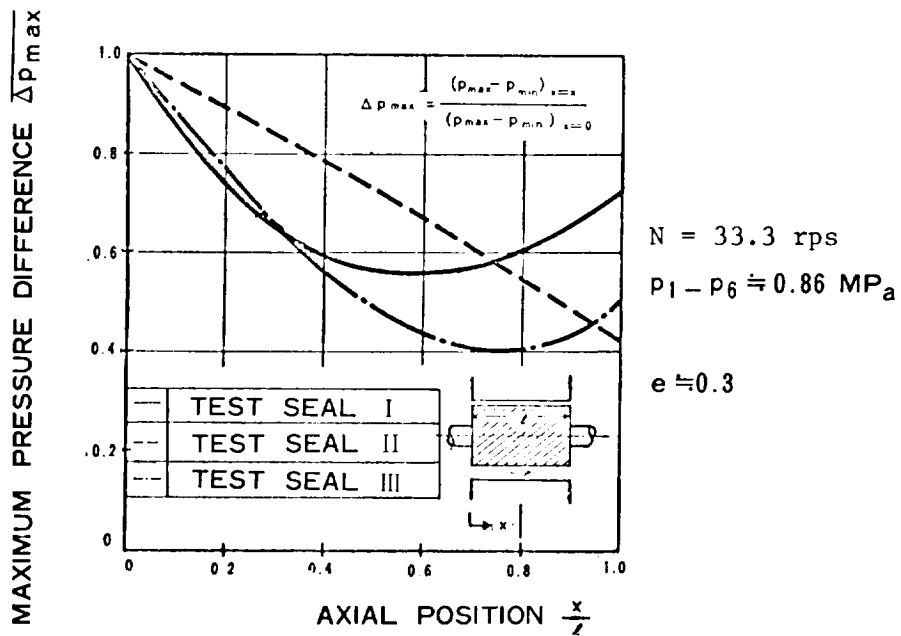


Figure 4. Change in circumferential pressure difference in the axial direction

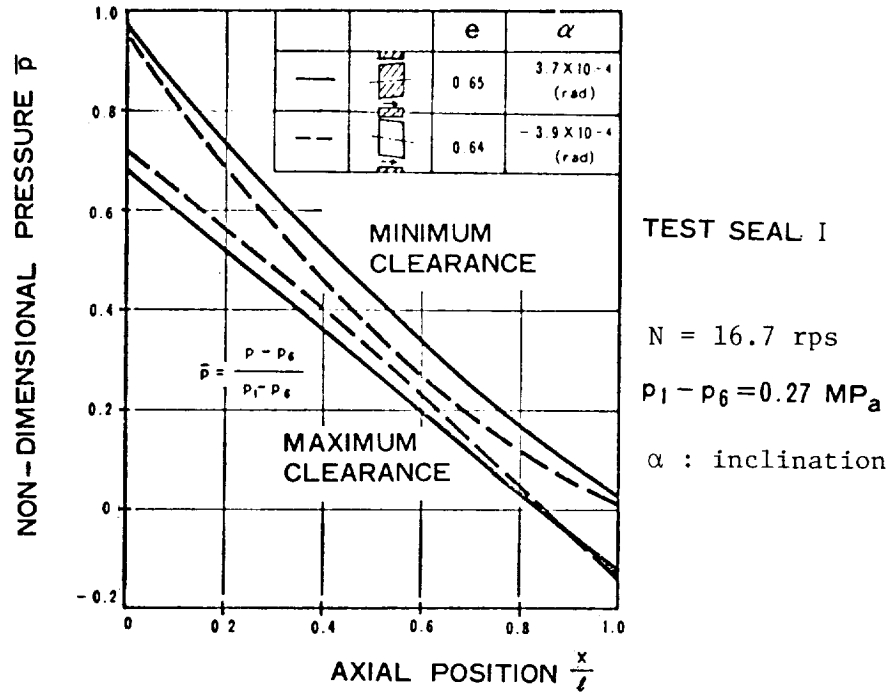


Figure 5. Pressure distribution in the axial direction
-Influence of inclination between rotor and stator axes

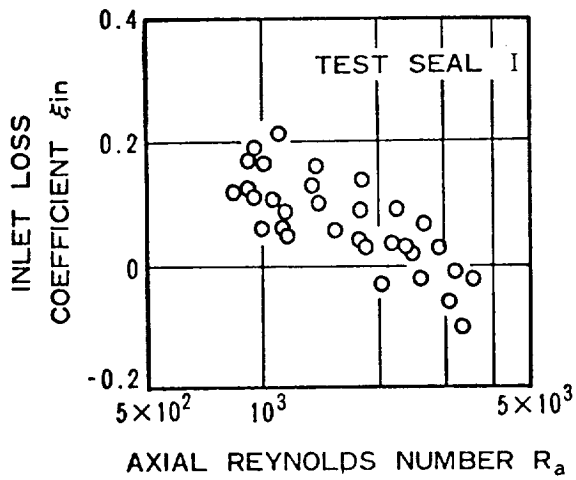


Figure 6. Inlet loss coefficient

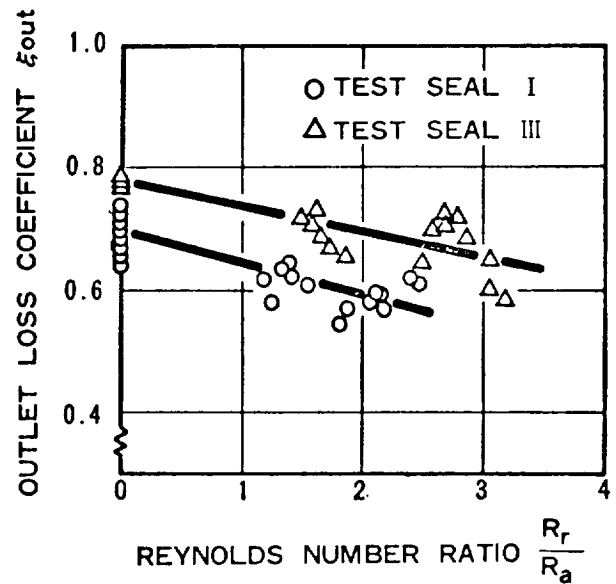


Figure 7. Exit loss coefficient

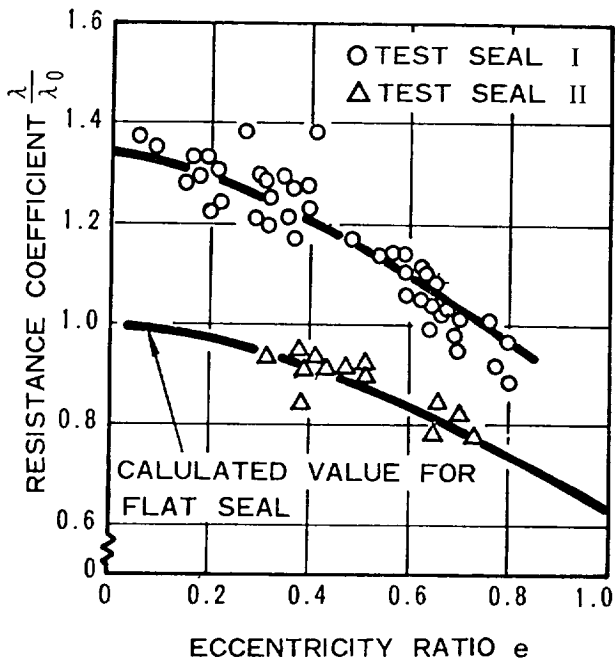


Figure 8. Resistance coefficient

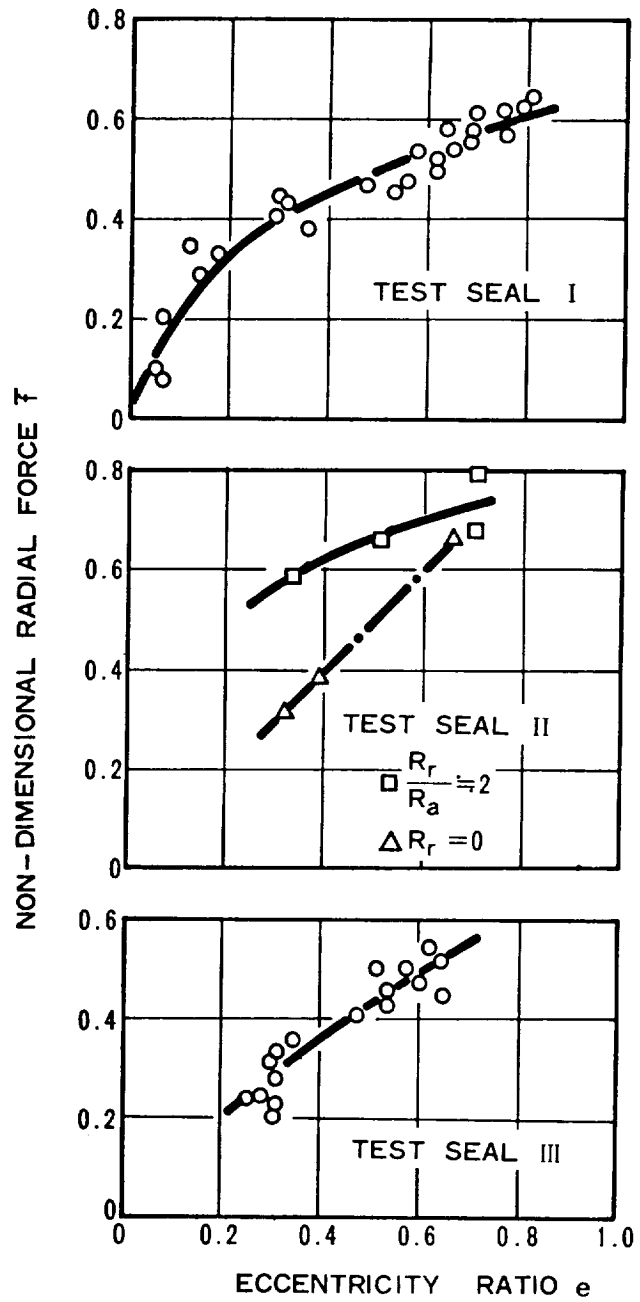


Figure 9. Radial force on the eccentric rotor

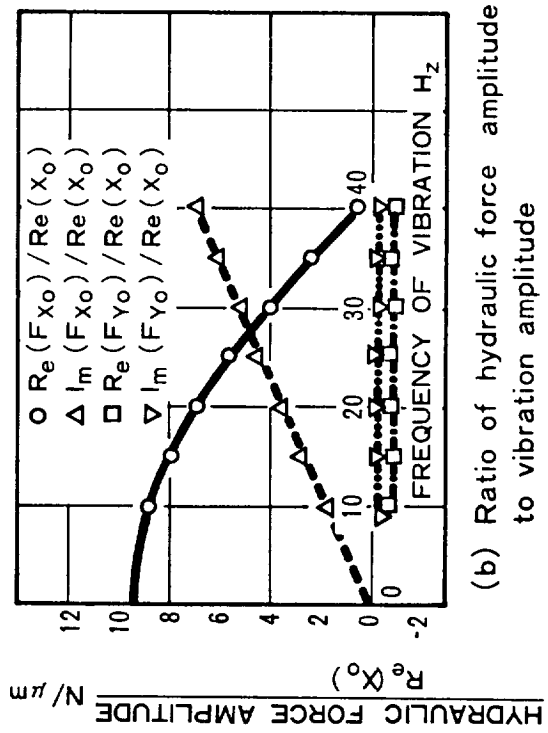
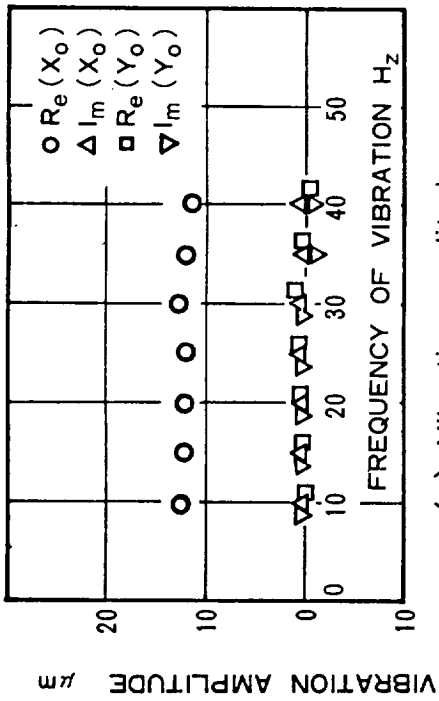


Figure 11. An example of experimental data

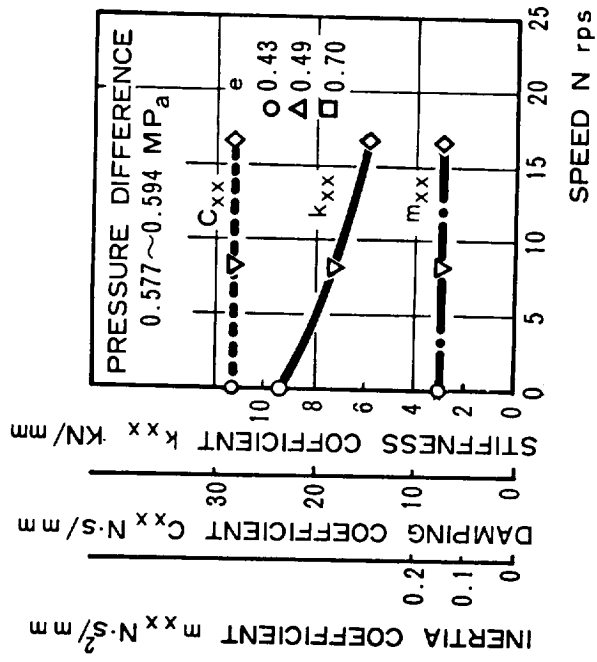


Figure 12. Test results of dynamic properties

